California Division of the American Cancer Society. A.T. is now supported by grants from the Swiss National Science Foundation and the Swiss Cancer League. Y.R. is a Merck fellow of the Life Sciences Research Foundation. This work was supported by the NIH (G.R.M. and J.M.B.), and the G.W. Hooper Foundation.

Competing interests statement

The authors declare that they have no competing financial interests.

Correspondence and requests for materials should be addressed to A.T. (e-mail: Andreas.Trumpp@isrec.unil.ch).

Bone indentation recovery time correlates with bond reforming time

James B. Thompson*, Johannes H. Kindt*, Barney Drake*, Helen G. Hansma*, Daniel E. Morse† & Paul K. Hansma*

** Department of Physics and † Department of Molecular, Cellular and Developmental Biology, University of California, Santa Barbara, California 93106, USA*

Despite centuries of work, dating back to Galileo[1], the molecular basis of bone's toughness and strength remains largely a mystery. A great deal is known about bone microstructure[2–5] and the microcracks[6,7] that are precursors to its fracture, but little is known about the basic mechanism for dissipating the energy of an impact to keep the bone from fracturing. Bone is a nanocomposite of hydroxyapatite crystals and an organic matrix. Because rigid crystals such as the hydroxyapatite crystals cannot dissipate much energy, the organic matrix, which is mainly collagen, must be involved. A reduction in the number of collagen cross links has been associated with reduced bone strength[8–10] and collagen is molecularly elongated ('pulled') when bovine tendon is strained[11]. Using an atomic force microscope[12–16], a molecular mechanistic origin for the remarkable toughness of another biocomposite material, abalone nacre, has been found[12]. Here we report that bone, like abalone nacre, contains polymers with 'sacrificial bonds' that both protect the polymer backbone and dissipate energy. The time needed for these sacrificial bonds to reform after pulling correlates with the time needed for bone to recover its toughness as measured by atomic force microscope indentation testing. We suggest that the sacrificial bonds found within or between collagen molecules may be partially responsible for the toughness of bone.

Such sacrificial bonds, in abalone nacre, are analogous to those in the muscle protein titin[13–16]. The energy needed to break a polymer designed in this way can be hundreds or even thousands of times greater than the energy needed to break a covalent bond, because the polymer must be re-stretched every time a sacrificial bond breaks and releases more 'hidden length'[13–16]. The hidden length can be, as in titin[13–16], the difference in length between an unfolded and a folded domain along one polymer chain or the extra length released when sacrificial bonds between two chains break.

Force versus extension curves—'pulls'—of collagen show that there are sacrificial bonds that can be broken, and thereby prevent the force from rising to a value that would break the collagen backbone (Fig. 1). If, after pulling on collagen, the tip of the atomic force microscope (AFM) is moved back to within approximately 50 nm of the surface, sacrificial bonds will reform. The longer the delay before the next pull, the more sacrificial bonds reform and thus the more energy dissipation observed when pulling the collagen molecule(s) again. If the collagen is in a calcium buffer, more sacrificial bonds reform and more energy dissipation is observed than if it is in a sodium buffer. Even so, less than half of the energy dissipation observed the first time collagen is pulled is regained by allowing a 100-s delay in calcium buffer. Energy dissipation also tends to decrease as collagen is repeatedly pulled, suggesting that either some of the sacrificial bonds cease to reform, or that one or more of several molecules attached to the tip become

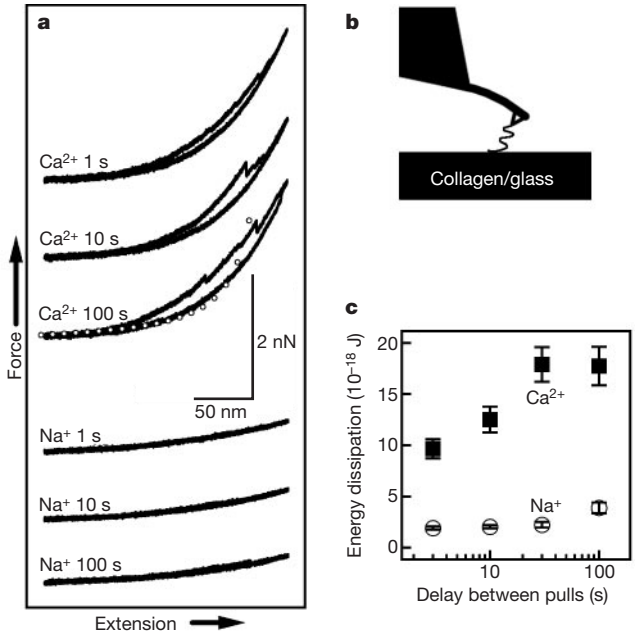

Figure 1 Pulling on collagen. **a**, Force versus extension curves obtained by pulling collagen molecules supported on a glass cover slip. The example curves shown were selected from a series of pulls on the same molecule(s) to have average values of energy dissipation, that is average areas enclosed by the extension away from the surface (upper trace) and return to the surface (lower trace). This energy dissipation changes with the delay between successive pulls, noted on the curves, on the same molecule(s). For calcium buffer, the area increases with delay. For sodium buffer, the area is smaller and increases less with delay. The return portion of the Ca^{2+} 100-s curve was fitted to the wormlike-chain model (open circles). The model does not fit well, suggesting that we are not puling on a single protein backbone. **b**, Diagram of the experiment. **c**, A plot of the average energy dissipation versus delay time. Each curve, Ca^{2+} and Na^{+}, was calculated from the enclosed area of several pulls on the same molecule(s).

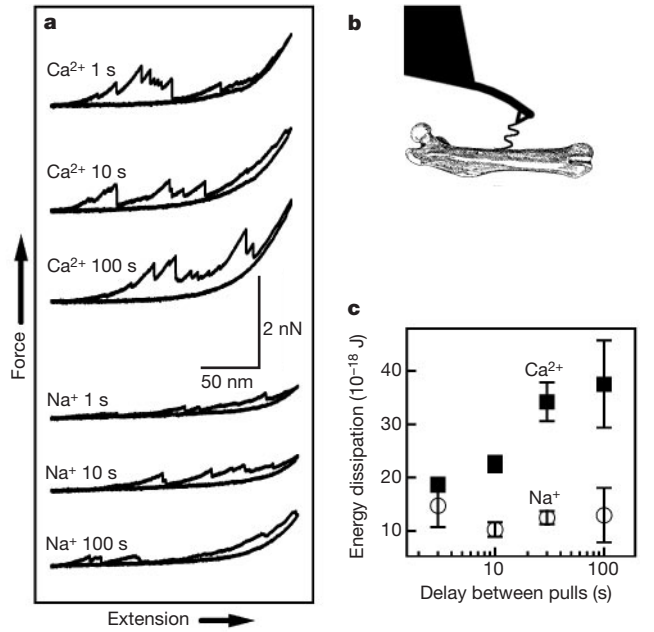

Figure 2 Pulling on bone. **a**, Force versus extension curves measured on a polished piece of fresh rat femur. **b**, Diagram of the experiment. **c**, As for Fig. 1c, measured on collagen, the energy dissipation measured on rat femur in a calcium buffer increases with the delay between pulls. We note that the timescale for this increase as a function of the delay between pulls is comparable to that in Fig. 1b.

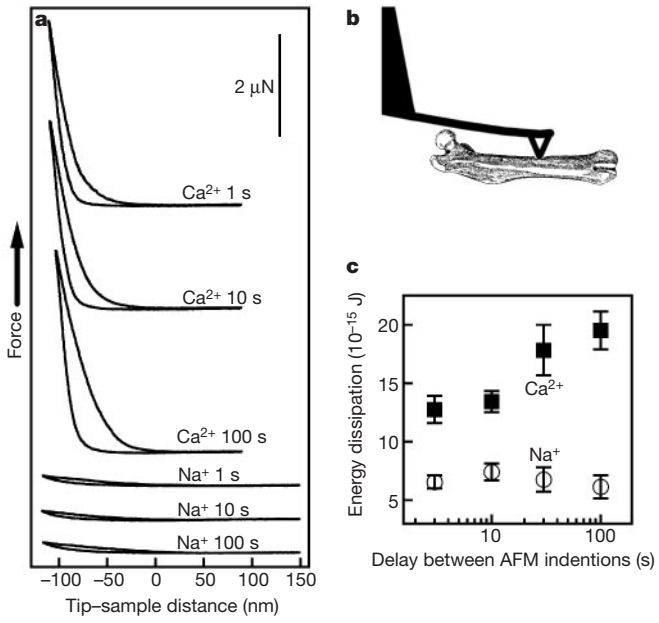

Figure 3 Indentation of bone. **a**, Non-destructive indentation curves on fresh rat femur probed at forces low enough that no permanent deformation of the surface occurs. In calcium buffer the bone is stronger, that is, the force versus tip sample distance curves are steeper. As in Figs 1 and 2, the area under the curves—energy dissipation—increases with increasing delay between indentations. **b**, Diagram of the experiment. **c**, Average energy dissipation versus delay time. The energy dissipation tends to be larger in calcium buffer and increases with a similar timescale to that observed in Figs 1 and 2. One major difference is that here the energy dissipation is roughly three orders of magnitude greater than in the molecular pulling curves even though the indentation distances are smaller than the pull distances. If the same molecules are involved, this implies that many more molecules are acting together to resist indentation than we 'pulled' in the pulling experiment.

detached. We do not know the nature of these sacrificial bonds. One possibility is that they include ionic bridges between two negatively charged ions on the collagen such as carboxylate ions. Divalent calcium ions can form such bridges, but monovalent sodium ions cannot.

Our collagen pulling data did not readily fit the wormlike-chain model[13,17] typically applied to pulling curves (Fig. 1). The fits implied persistence lengths of only 0.03 nm. Such a persistence length is unphysical and less than a tenth of the value typically quoted for pulling on single proteins[13–15]. Either we are pulling on several molecules in parallel, or collagen has unusual force versus extension properties. The collagen backbone is folded into a triple helix, which might not become unfolded during extension. Therefore, when pulling collagen, we might be stretching three interacting protein chains, even when pulling on a single molecule. If so, the wormlike chain would be an inappropriate model for pulling curves on collagen.

This research on pulling collagen complements existing research on collagen with AFMs. After early pioneering papers[18,19] there have been over thirty papers reporting the use of AFM to image collagen from sources as diverse as tendon[20], dentin[21] and cornea[22,23]. Both assembly[22,24] and degradation have been studied[25,26]. Pulling curves on collagen have also been reported[27], but the ability of collagen to recover energy dissipation with time was not investigated.

It is not necessary to use purified collagen to observe the behaviour shown in Fig. 1. Similar behaviour is seen when pulling molecules exposed on a polished bone (rat femur) surface (Fig. 2). At this time, we cannot prove that these pulling curves are due to pulling of collagen. However, pulling curves for polished bone are similar to those for purified collagen and exhibit a similar recovery of energy dissipation as a function of the delay between pulls, suggesting that we are pulling on similar molecules in both cases. Further, collagen is the most abundant polymer found in bone and we find the behaviour shown in Fig. 2 to be ubiquitous on the surface of bone.

We wondered whether this mechanism of energy dissipation has any relationship to energy dissipation or strength in bone. Our first experiment in this area involved soaking bovine femur samples with dimensions of order 2 cm × 2 mm × 2 mm in either 1 M NaCl or 1 M $CaCl_2$ for several days and then performing four point bending tests. These tests showed that the yield strength of samples soaked in 1 M $CaCl_2$ was not significantly different than the yield strength of samples soaked in 1 M NaCl. Thus, we were led to the conclusion that either this mechanism of energy dissipation had nothing to do with the yield strength of bone, or that the ions in our two solutions had not completely penetrated our samples and exchanged with the ions already present.

In an attempt to determine which was the correct answer, we tried a more local probe of the strength and toughness of bone. We used a very stiff AFM cantilever (50 N m^{-1}) to indent rat femur samples, and found significant differences between samples soaked in calcium buffer and those soaked in sodium buffer (Fig. 3). On average, samples soaked in calcium buffer appeared harder, and when they were indented by about 50 nm these samples recovered their initial energy dissipation with a similar timescale to that observed in collagen. It is important to note that indenting the bone surface by about 50 nm did not produce a permanent deformation, which suggests that the bone's structure was not greatly altered. When the surface was indented by about 100 nm, a permanent deformation of the surface occurred, and energy dissipation did not recover within 100 s. AFM indentation is only sensitive to changes of bone properties near the surface, yet we found it necessary to soak bone samples for a day or more before they reached steady-state properties. It appears that the exchange of ions is slow within bone, which supports the hypothesis that our macroscopic bone tests showed no differences owing to insufficient penetration and exchange of the solution ions with those buried in the bone. It has been found that AFM indentation of primary osteoblasts results in increased intracellular calcium concentration[28].

For sacrificial bonds in collagen to dissipate energy during

indentation, indentation must result in sufficient elongation of collagen to break these sacrificial bonds. We do not yet understand how this occurs. Collagen within bone is assembled into fibrils[2–4] and thereby held in an extended configuration. We speculate that collagen in this extended configuration may be pre-stressed so that sacrificial bonds must be broken in order to allow even small indentations in the bone surface.

It seems surprising that bonds may form at the same rate within collagen supported on a glass slide and collagen in bone. Perhaps the formation of sacrificial bonds requires only the presence of multivalent ions, which bind two sites on the same or (more probably) two different collagen molecules. Solution ions were given several days to penetrate the bone samples, so the concentration of multivalent ions within the outer layers of the bone samples should be similar to that seen by collagen molecules exposed directly to the solution.

Thus, we have shown that in bone that has been indented, in molecules from bone that have been pulled and in purified collagen that has been pulled, the recovery of toughness takes about the same amount of time. This correlation in time dependence suggests, but does not prove, that these recoveries may be related. The recovery of toughness in our pulling experiments is in some ways similar to that seen in experiments on abalone shell proteins[12] and titin[13–16]. Although there are almost certainly not any precisely folded domains as in titin, there do appear to be renewable sacrificial bonds that break at forces below the force needed to break the backbone of these polymers. These sacrificial bonds provide a mechanism for toughness; it takes much more energy to pull these molecules than it would in the absence of sacrificial bonds. This property of collagen is of interest because collagen is the most abundant protein in the human body and serves as a structural component of a variety of tissues including bone, tendon, and skin.

Note added in proof: Initial experiments indicate that pulling curves taken on collagen molecules in PBS also show a recovery of energy dissipation with time delay between pulls (our own unpublished data). Thus, multivalent negative ions, such as phosphate, also appear to form sacrificial bonds. □

Methods

AFM pulling

The pulling experiments were conducted using a prototype small-cantilever AFM. The cantilevers used typically had spring constants of 50 pN nm^{-1}, resonant frequencies of 120 kHz and 0.5-μm-long electron-beam-deposited tips. Coating the cantilever tip with gold did not affect the results reported. The pulling curves shown were taken with a 30-kHz bandwidth and at a loading rate of 2 μm s^{-1}. Our typical root mean square (r.m.s.) noise level was less than 0.3 pN $Hz^{-1/2}$. The force was measured by multiplying the deflection of the cantilever by the spring constant of the cantilever. Extension is measured from the starting point of the pulls: approximately 50 nm off the surfaces. During each pull the molecules were extended by 200 nm. Pulling curves were captured in a series with 1-s delays between pulls of: 1, 1, 100, 1, 30, 1, 10, 1, 3, 1, 3, 1, 10, 1, 30, 1, 100, 1, 100, 1, 30, 1, 10, 1, 3, 1, 3, 1, 10, 1, 30, 1 and 100 seconds (in that order), without contacting the surface. The tip was kept approximately 50 nm away from the surface during the entire series to avoid picking up additional molecules. Energy dissipation was calculated and averaged for all curves in a single series to produce the data sets shown in Figs 1b and 2b.

AFM indentation

The AFM indentation tests were conducted using a commercial atomic force microscope (Nanoscope III MultiMode from Digital Instruments) and cantilever (Nanosensors). These curves were taken over a 2-s period. The surface was typically raised 50 nm beyond the point where the cantilever first made contact, but it was necessary to reduce this distance on particularly hard samples. Force was calculated by multiplying cantilever deflection by the spring constant of the cantilever, in this case approximately 50 N m^{-1}. Tip sample distance refers to the motion of the sample, which is raised for the indention, minus the deflection of the cantilever. Positive tip–sample distances correspond to the tip being above the surface of the sample. Negative tip–sample distances correspond to the tip indenting below the original surface of the sample ('zero'). Indentation curves were captured in a series with delays between indentations of either: 1, 1, 100, 1, 30, 1, 10 and 3 s or the reverse order (increasing from 3 to 100 s). Energy dissipation was calculated and averaged for curves taken at five or more positions, separated from each other by 20 μm, on the bone surface to produce the data sets shown in Fig. 3b.

Buffers

Each measurement was conducted in one of two buffers. The calcium buffer contained 40 mM $CaCl_2$, 110 mM NaCl, and 10 mM HEPES. The sodium buffer contained 150 mM NaCl and 10 mM HEPES. The pH of both solutions was adjusted to 7.0 using a small amount of NaOH.

Collagen sample preparation

Collagen samples were prepared by suspending ~1 mg of acid insoluble collagen from bovine Achilles tendon (Sigma)[29] in a 10 μl drop of PBS (phosphate buffered saline) on a cover glass. A second cover glass was used to shear the collagen on the first cover glass. The PBS was then allowed to evaporate to dryness. The dried sample was rinsed under a stream of deionized water (Milli-Q) for 15 s before placing either sodium or calcium buffer on the sample and introducing it into the AFM.

Bone sample preparation

The bone samples used in the pulling and indentation experiments were prepared from the mid-section of a rat femur. The rat had been killed less than 1 h before sample preparation. The femur was first cleaned and cut into pieces of about 2 mm × 2 mm × 0.5 mm. The 2 mm × 2 mm surface was sanded with 400 grit and then 600 grit silicon carbide sandpaper. After sanding, the surface was polished with 30 μm, 6 μm, 1 μm and finally 0.25 μm diamond suspensions before thoroughly rinsing it in Milli-Q water. This left a clean, flat surface of longitudinally cut compact bone. The samples were stored under buffer. The pulling curves shown were taken on the first and second day after sample preparation. The samples were soaked in the buffer solutions at 6 °C for 5 days before AFM indentation testing.

Received 29 August; accepted 4 October 2001.

1. Ascenzi, A. Biomechanics and Galileo Galilei. *J. Biomech.* **26,** 95–100 (1993).
2. Weiner, S. & Wagner, H. D. The material bone: structure-mechanical function relations. *Annu. Rev. Mater. Sci.* **28,** 271–298 (1998).
3. Weiner, S., Traub, W. & Wagner, H. D. Lamellar bone: structure-function relations. *J. Struct. Biol.* **126,** 241–255 (1999).
4. An, Y. H. & Draughn, R. A. *Mechanical Testing of Bone and the Bone–Implant Interface* (CRC Press, New York, 2000).
5. Currey, J. D. *The Mechanical Adaptations of Bones* (Princeton Univ. Press, Princeton, 1984).
6. Reilly, G. C. & Currey, J. D. The effects of damage and microcracking on the impact strength of bone. *J. Biomech.* **33,** 337–343 (2000).
7. Reilly, G. C. & Currey, J. D. The development of microcracking and failure in bone depends on the loading mode to which it is adapted. *J. Exp. Biol.* **202,** 543–552 (1999).
8. Oxlund, H., Barckman, M., Ortoft, G. & Andreassen, T. T. Reduced concentrations of collagen cross-links are associated with reduced strength of bone. *Bone* **17,** S365–S371 (1995).
9. Burstein, A. H., Zika, J. M., Heiple, K. G. & Klein, L. Contribution of collagen and mineral to the elastic–plastic properties of bone. *J. Bone Joint Surg. A* **57,** 956–961 (1975).
10. Knott, L. & Bailey, A J. Collagen cross-links in mineralizing tissues: A review of their chemistry, function, and clinical relevance. *Bone* **22,** 181–187 (1998).
11. Sasaki, N. & Odajima, S. Elongation mechanism of collagen fibrils and force–strain relations of tendon at each level of structural hierarchy. *J. Biomech.* **29,** 1131–1136 (1996).
12. Smith, B. L. *et al.* Molecular mechanistic origin of toughness of natural adhesives, fibre and composites. *Nature* **399,** 761–763 (1999).
13. Rief, M., Gautel, M., Oesterhelt, F., Fernandez, J. M. & Gaub, H. E. Reversible unfolding of individual titin immunoglobulin domains by AFM. *Science* **276,** 1109–1112 (1997).
14. Rief, M., Gautel, M., Schemmel, A. & Gaub, H. E. The mechanical stability of immunoglobulin and fibronectin II domains in the muscle protein titin measured by atomic force microscopy. *Biophys. J.* **75,** 3008–3014 (1998).
15. Li, H., Oberhauser, A. F., Fowler, S. B., Clarke, J. & Fernandez, J. M. Atomic force microscopy reveals the mechanical design of a modular protein. *Proc. Natl Acad. Sci. USA* **97,** 6527–6531 (2000).
16. Oberhauser, A. F., Hansma, P. K., Carrion-Vazquez, M. & Fernandez, J. M. Stepwise unfolding of titin under force-clamp atomic force microscopy. *Proc. Natl Acad. Sci. USA* **98,** 468–472 (2001).
17. Bustamante, C., Marko, J. F., Siggia, E. D. & Smith, S. Entropic elasticity of lambda-phage DNA. *Science* **265,** 1599–1600 (1994).
18. Chernoff, E. A. G. & Chernoff, D. A. Atomic force microscope images of collagen fibers. *J. Vac. Sci. Technol. A* **10,** 596–599 (1994).
19. Revenko, I., Sommer, F., Minh, D. T., Garrone, R. & Franc, J. M. Atomic force microscopy study of the collagen fiber structure. *Biol. Cell* **80,** 67–69 (1994).
20. Bigi, A., Gandolfi, M., Roveri, N. & Valdre, G. *In vitro* calcified tendon collagen: an atomic force and scanning electron microscopy investigation. *Biomaterials* **18,** 657–665 (1997).
21. El Feninat, F., Ellis, T. H., Sacher, E. & Stangel, I. Moisture-dependent renaturation of collagen in phosphoric acid etched human dentin. *J. Biomed. Mater. Res.* **42,** 549–553 (1998).
22. Miyagawa, A. *et al.* Surface topology of collagen fibrils associated with proteoglycans in mouse cornea and sclera. *Jpn J. Ophthalmol.* **44,** 591–595 (2000).
23. Fullwood, N. J., Hammiche, A., Pollock, H. M., Hourston, D. J. & Song, M. Atomic force microscopy of the cornea and sclera. *Curr. Eye Res.* **14,** 529–535 (1995).
24. Paige, M. F. & Goh, M. C. Ultrastructure and assembly of segmental long spacing collagen studied by atomic force microscopy. *Micron* **32,** 355–361 (2001).
25. Lin, H., Clegg, D. O. & Lal, R. Imaging real-time proteolysis of single collagen I molecules with an atomic force microscope. *Biochemistry* **38,** 9956–9963 (1999).
26. Yamamoto, S. *et al.* The subfibrillar arrangement of corneal and scleral collagen fibrils as revealed by scanning electron and atomic force microscopy. *Arch. Histol. Cytol.* **63,** 127–135 (2000).
27. Dufrene, Y. F., Marchal, T. G. & Rouxhet, P. G. Influence of substratum surface properties of the organization of adsorbed collagen films: *in situ* characterization by atomic force microscopy. *Langmuir* **15,** 2871–2878 (1999).
28. Charras, G. T., Lehenkari, P. P. & Horton, M. A. Atomic force microscopy can be used to mechanically stimulate osteoblasts and evaluate cellular strain distributions. *Ultramicroscopy* **86,** 86–95 (2001).
29. Einbinder, J. & Schubert, M. Binding of mucopolysaccharides and dyes by collagen. *J. Biol. Chem.* **188,** 335–341 (1951).
30. Greene, E. C. *Anatomy of the Rat* (Hafner, New York, 1963).

Acknowledgements

We thank E. Oroudjev, J. Cooper, D. Kohn and L. Fisher for their assistance and discussion. We also thank the reviewers of our paper for their helpful suggestions. We thank S. Babbitt and the American Philosophical Society for granting us permission to use the drawing of a rat femur[30] shown in Figs 2 and 3. This work was supported by the Materials Research Division and MCB Division of the National Science Foundation, the Materials Research Laboratory Program of the National Science Foundation, and the MURI programme of the Army Research Office.

Correspondence and requests for materials should be addressed to J.B.T. (e-mail: jbthomp@physics.ucsb.edu).

Bacteriophytochromes are photochromic histidine kinases using a biliverdin chromophore

Seong-Hee Bhoo*†, Seth J. Davis*†‡, Joseph Walker*, Baruch Karniol* & Richard D. Vierstra*

** Cellular and Molecular Biology Program and the Department of Horticulture, University of Wisconsin—Madison, 1575 Linden Drive, Madison, Wisconsin 53706, USA*

† These authors contributed equally to this work

Phytochromes comprise a principal family of red/far-red light sensors in plants[1]. Although phytochromes were thought originally to be confined to photosynthetic organisms[2,3], we have recently detected phytochrome-like proteins in two heterotrophic eubacteria, *Deinococcus radiodurans* and *Pseudomonas aeruginosa*[4]. Here we show that these form part of a widespread family of bacteriophytochromes (BphPs) with homology to two-component sensor histidine kinases. Whereas plant phytochromes use phytochromobilin as the chromophore, BphPs assemble with biliverdin, an immediate breakdown product of haem, to generate photochromic kinases that are modulated by red and far-red light. In some cases, a unique haem oxygenase responsible for the synthesis of biliverdin is part of the BphP operon. Co-expression of this oxygenase with a BphP apoprotein and a haem source is sufficient to assemble holo-BphP *in vivo*. Both their presence in many diverse bacteria and their simplified assembly with biliverdin suggest that BphPs are the progenitors of phytochrome-type photoreceptors.

Photosynthetic organisms use an array of photoreceptor systems to optimize their growth and development to the ambient light environment. The phytochromes of plants form a family of homodimeric chromoproteins, which contain the linear tetrapyrrole 3E-phytochromobilin (PΦB) covalently attached to polypeptides of about 1,100 amino acids[1]. These photoreceptors sense red (R) and far-red (FR) light through photo-interconversion between two stable conformations, an R-absorbing Pr form, and an FR-absorbing Pfr form. Because Pfr is biologically active but Pr is inactive, phytochromes act as reversible R/FR 'switches' that synchronize many aspects of photomorphogenesis[1].

We have identified strong sequence homology between the previously reported phytochrome-like proteins from *D. radiodurans* and *P. aeruginosa*[4] and the *BphP* loci from the Gram-negative bacteria *Pseudomonas syringae* strain DC3000, *Pseudomonas putida*, *Pseudomonas fluorescens*, *Agrobacterium tumefaciens* and *Rhizobium leguminosarium*, the α-proteobacterium *Rhodobacter sphaeroides*, the previously described phytochrome-like photoreceptors from the α-proteobacterium *Rhodospirillum centenum*[5] and several cyanobacteria[6,7], and BphP-like sequences from the fungi *Neurospora crassa* and *Aspergillus fumigatus* (Fig. 1a). Like phytochromes, these bacteriophytochrome photoreceptors (BphPs) contain an amino-terminal chromophore-binding domain, which autocatalytically attaches bilins, followed by a histidine kinase module[3,4]. BphPs are notably distinct from phytochromes as they lack the cysteine used by phytochromes to bind bilins through a thioether bond[1]. Instead, BphPs seem to use the adjacent conserved histidine to bind the bilin through a Schiff-base-type linkage (ref. 4; and Fig. 1a). This protein organization suggested that BphPs, like cyanobacterial phytochromes[8,9], function as light-activated kinases similar to other bacterial two-component sensors[10].

Whereas higher plant and cyanobacterial phytochromes are known to use respectively PΦB and 3Z-phycocyanobilin (PCB) as the chromophore[1,9], the chromophore of BphP was unclear because bacteria other than cyanobacteria and fungi are not known to produce such linear bilins[11]. To determine whether the BphP chromophore is a bilin, we isolated the native BphP photoreceptor from wild-type *D. radiodurans* and assayed it for this type of chromophore by zinc-induced fluorescence[12]. To enrich for *Dr* BphP, we used anti-*Dr* BphP antibodies to concentrate it directly from a crude soluble lysate. The enriched protein fluoresced in the presence of zinc and ultraviolet light similar to holo-BphP

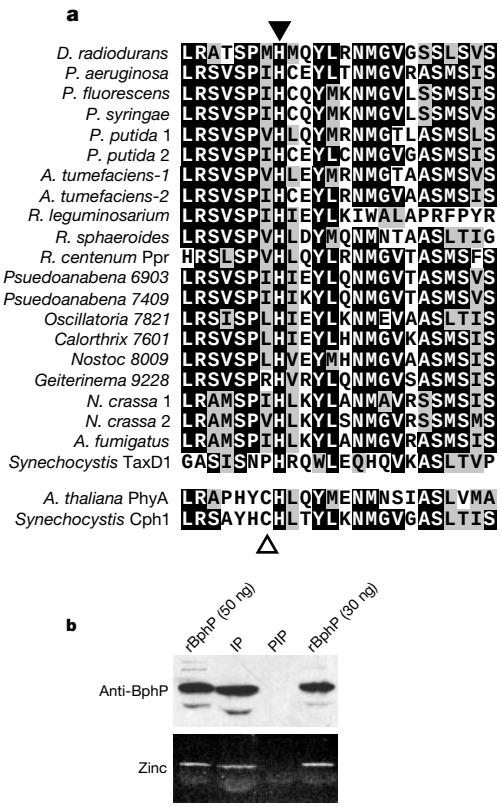

Figure 1 Sequence comparison of the BphP family and detection of the BphP chromoprotein from *D. radiodurans*. **a**, Amino-acid sequence alignment of the region surrounding the predicted chromophore-binding site for BphPs and phytochromes. Filled and open arrowhead identifies the histidine and cysteine residue involved in binding the bilin in BphPs and the phytochromes (*A. thaliana* phyA and *Synechocystis* Cph1), respectively. Reverse type and grey boxes denote identical and similar amino acids, respectively. **b**, Detection of BphP from *D. radiodurans*. *Dr* BphP was immuno-affinity purified from crude cell extracts with either anti-*Dr* BphP antibodies (IP) or pre-immune serum (PIP) and subject to SDS–PAGE. The polypeptide was detected by immunoblot analysis with anti-*Dr* BphP antibodies, and the bound bilin chromophore was detected by zinc-induced fluorescence. *Dr* BphP bound to BV *in vitro* was used as a standard.

‡ Present address: Department of Biological Sciences, University of Warwick, Coventry CV4 7AL, UK.